Neuroinflammation Appears Early on PET Imaging and Then Plateaus in a Mouse Model of Alzheimer Disease

Francisco R. López-Picón[1,2], Anniina Snellman[1,2], Olli Eskola[3], Semi Helin[3], Olof Solin[3–5], Merja Haaparanta-Solin[1,2], and Juha O. Rinne[6,7]

[1]Preclinical Imaging, Turku PET Centre, University of Turku, Turku, Finland; [2]MediCity Research Laboratory, University of Turku, Turku, Finland; [3]Radiopharmaceutical Chemistry Laboratory, Turku PET Centre, University of Turku, Turku, Finland; [4]Department of Chemistry, University of Turku, Turku, Finland; [5]Accelerator Laboratory, Åbo Akademi University, Turku, Finland; [6]Turku PET Centre, Turku University Hospital, Turku, Finland; and [7]Division of Clinical Neurosciences, Turku University Hospital, Turku, Finland

Neuroinflammation has been associated with various neurologic diseases, including Alzheimer disease (AD). In AD, the translocator protein 18 kDa (TSPO) is overexpressed in the activated microglia that surround the β-amyloid plaques. In the current longitudinal study using a mouse model of AD, we evaluated the association between β-amyloid deposition and neuroinflammation in AD. **Methods:** To monitor the longitudinal changes in β-amyloid deposition and neuroinflammation, we used in vivo PET imaging and ex vivo autoradiography with Pittsburgh compound B (^{11}C-PIB) and a TSPO tracer, flutriciclamide (^{18}F-GE-180), in the APP23 mouse model of AD. We also applied immunohistochemistry to study β-amyloid and activated microglia in the mouse brain tissue. **Results:** From 17 to 26 mo of age, the mice showed robust increased binding of ^{11}C-PIB with aging in the frontal cortex, parietotemporal cortex, hippocampus, and thalamus whereas the increase in ^{18}F-GE-180 binding with aging was minimal in areas of early amyloidosis such as the frontal cortex and hippocampus. A clear positive correlation between β-amyloid deposition and neuroinflammation was detected with ^{11}C-PIB and ^{18}F-GE-180 only in the parietotemporal cortex and thalamus. **Conclusion:** The neuroinflammation increase detected with ^{18}F-GE-180 is less than the increase in amyloidosis detected with ^{11}C-PIB. Furthermore, binding of ^{18}F-GE-180 plateaus at an earlier stage of pathogenesis whereas amyloidosis continues to increase. We suggest that TSPO can be a good marker for early pathogenesis detection but not for tracking long-term disease progression.

Key Words: Alzheimer disease; neuroinflammation; β-amyloid; GE-180; PIB

Many of the pathologic hallmarks of Alzheimer disease (AD), such as β-amyloid deposition, neuroinflammation, and changes in different neurotransmitter systems and glucose metabolism, can be investigated noninvasively using PET. PET allows both investigation of the pathologic processes and diagnosis and evaluation of the efficacy of AD treatments (1,2). Pittsburgh compound B (^{11}C-PIB), the most used amyloid radioligand in PET studies of AD, enables the in vivo detection of Aβ-deposits in the human brain (3–5) and in some animal models (6–10).

Neuroinflammation caused by microglial activation has been suggested as an important factor affecting cognitive decline in AD (11) and as a pathologic event. Pathologic triggers activate microglia, which migrate to the injury site, initiating an innate immune response. The microglial activation increases expression of the mitochondrial 18-kDa translocator protein (TSPO), which has been the main target for in vivo PET imaging ligands for neuroinflammation with various radiotracers, including ^{11}C-PK-11195, ^{11}C-PBR28, ^{11}C-AC5216, ^{18}F-PBR06, ^{18}F-DPA-714, and ^{18}F-GE-180 (12–17).

^{18}F-GE-180 (flutriciclamide) is a novel high-affinity fluorinated TSPO-binding radiotracer (18). In recent studies, ^{18}F-GE-180 showed higher binding affinity than ^{11}C-PK-11195 in a rat model of stroke (19) and in acute neuroinflammation (20,21). This tracer also has been used to study microglial activation in an animal model of multiple sclerosis (22) and in the APPswe-PS1dE9 and PS2APP mouse models of AD (17,23). Furthermore, the first kinetic analysis in the human brain in healthy subjects has been performed (24).

In this study, we assessed the association of β-amyloid deposition and neuroinflammation in a longitudinal study using ^{11}C-PIB and ^{18}F-GE-180 in the APP23 mouse model of AD.

MATERIALS AND METHODS

Tracer Synthesis

[11]C-PIB and ^{18}F-GE-180 were synthesized at the Radiopharmaceutical Chemistry Laboratory of Turku PET Centre. For ^{11}C-PIB, desmethyl-PIB was labeled with ^{11}C-methyl triflate, produced from ^{11}C-CO$_2$. ^{11}C-PIB was formulated for injection in propylene glycol/ethanol/0.1 M phosphate buffer (2:1:14, v:v:v). The radiochemical purity exceeded 95% in all syntheses ($n = 25$).

^{18}F-GE-180 was synthesized according to a previously published method (25). The molar activity of ^{18}F-GE-180 was 2.0 ± 0.5 TBq/μmol at the end of synthesis ($n = 13$). Radiochemical purity was at least 98%.

Animals

All animal experiments were approved by the Regional State Administrative Agency for Southern Finland (ESAVI/4499/04.10.07/2016 and ESAVI/3899/04.10.07/2013). APP23 mice ($n = 36$; 30 female and 6 male) (Novartis Inc.) express human APP751swe driven by the

neuron-specific mouse Thy-1.2 gene fragment as a promoter. Aβ-immunoreactive plaques develop progressively in the neocortex and hippocampus and are associated with dystrophic neurites and gliosis (26,27). All animals were group-housed under standard conditions (temperature, 21°C ± 3°C; humidity, 55% ± 15%; lights on from 6:00 A.M. until 6:00 P.M.) and had ad libitum soy-free chow (RM3 (E) soya-free, 801710; Special Diet Services) and tap water.

In Vivo Binding of ^{11}C-PIB and ^{18}F-GE-180

The in vivo pilot study was performed with 6 transgenic and 6 wild-type (WT) 26-mo-old mice. Both groups were studied using ^{11}C-PIB and ^{18}F-GE-180.

The in vivo longitudinal study from 17 to 23 mo of age started with 5 transgenic and 6 WT mice. Both groups were studied using ^{11}C-PIB and ^{18}F-GE-180. These mice were imaged at 17, 20, and 23 mo of age.

The mice were anesthetized with a 2.5% isoflurane–oxygen mixture 30 min before injection and then were injected intravenously with either ^{11}C-PIB (injected dose, 10.05 ± 0.87 MBq) or ^{18}F-GE-180 (injected dose, 10 ± 0.65 MBq) for scanning by an Inveon multimodality PET/CT scanner (Siemens Medical Solutions). A few drops of Oftagel (2.5 mg/g; Santen) were applied to the eyes of the animals to prevent eye dryness. The scanner has a 12.7-cm axial field of view and a 10-cm transaxial field of view, generating images from 159 transaxial slices. The mice were scanned for 10 min with CT for attenuation correction and anatomic reference, and immediately afterward the tracer was injected and a 60-min dynamic PET scan was started (51 frames: 30 × 10s, 15 × 60s, 4 × 300, and 2 × 600 s).

Analysis of PET Data

Image registration and analysis were performed using Inveon Research Workplace, version 3.0 (Siemens Medical Solutions). The dynamic PET images were coregistered with the CT images using the first 12 frames of the PET scan (2 min), and automatic rigid registration was applied. Registration was always assessed and manually corrected if needed. Afterward, the PET/CT images were manually coregistered with an averaged mouse MRI template, and standardized volumes of interest were placed in the frontal cortex (FC), parietotemporal cortex (PTC), cerebellum, hippocampus, and thalamus using the template as an anatomic reference (28). Different brain region volume-of-interest–to–cerebellum ratios were calculated for the late washout phase (50–60 min). Also, SUVs were calculated for the cerebellum to study changes over time in order to validate its use as a reference region (Supplemental Fig. 1; supplemental materials are available at http://jnm.snmjournals.org).

Ex Vivo Binding of ^{11}C-PIB– and ^{18}F-GE-180–Derived Radioactivity in Mouse Brain

For the ex vivo studies with ^{11}C-PIB, 6 WT and 6 transgenic 26-mo-old mice were used (injected dose, 10.3 ± 1.0 MBq); for the ex vivo studies with ^{18}F-GE-180, 4 WT and 6 transgenic 26-mo-old mice were used (injected dose, 10 ± 0.9 MBq). The mice lay on a heating pad and were kept under 2.5% isoflurane–oxygen anesthesia during the study.

The mice were sacrificed with cardiac puncture under deep anesthesia 10 min after ^{11}C-PIB injection or 60 min after ^{18}F-GE-180 injection. The whole intact brain was dissected and weighed, and the radioactivity in the brain was measured in the γ-counter (Wizard^2 3″; PerkinElmer). The brain was then quickly frozen in isopentane (2-methylbutane; Sigma-Aldrich) on dry ice. Ten to sixteen coronal sections (20 μm thick) per studied area from each brain were obtained using a cryomicrotome (Leica CM3050S) and collected on a glass slide (Superfrost Ultra Plus; Thermo Fisher). The slides were exposed to an image plate (Fuji BAS Imaging Plate TR2025; Fuji Photo Film Co., Ltd.) for about 2 half-lives of the radioisotope in question.

After the exposure, the imaging plates were scanned using a BAS-5000 reader (Fuji) with a resolution of 25 μm, and the saved images on
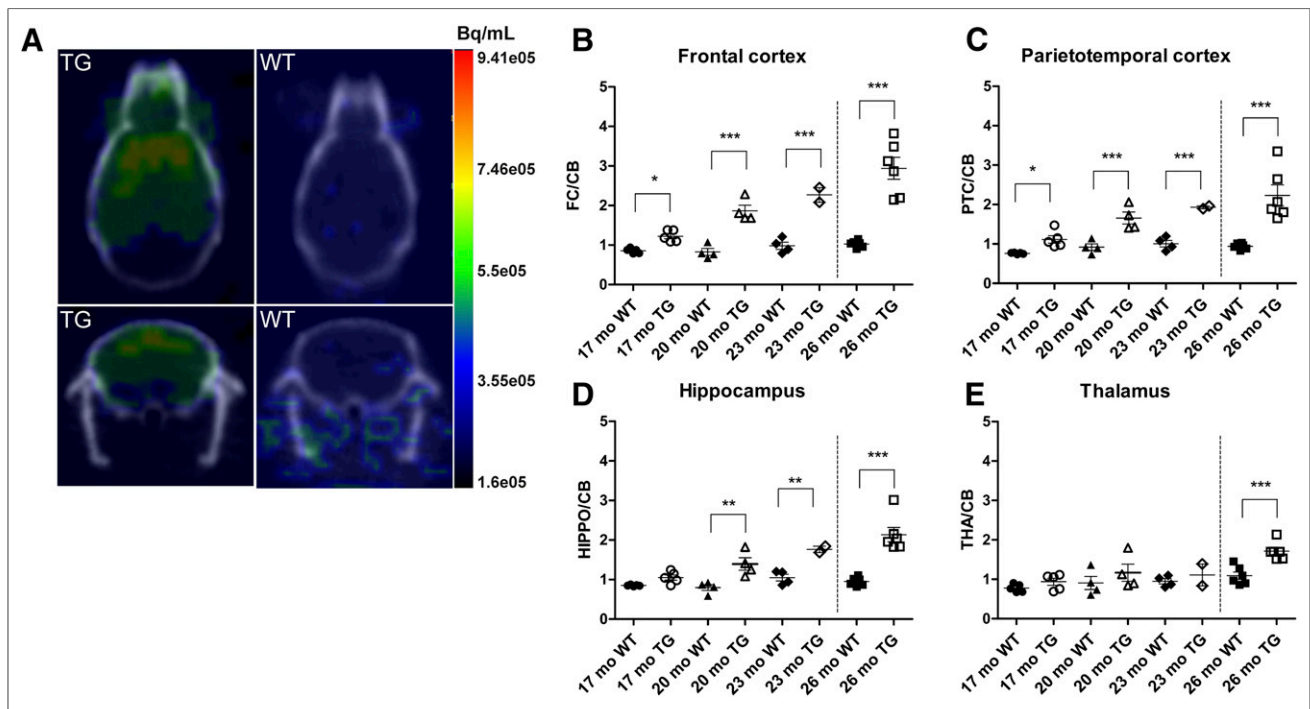

FIGURE 1. (A) In vivo PET images of ^{11}C-PIB in 26-mo-old transgenic (TG) and WT APP23 mice. (B–E) Ratios of FC (B), PTC (C), hippocampus (HIPPO) (D), and thalamus (THA) (E) to cerebellum (CB) from 17 to 26 mo of age. Dotted line separates data of pilot study from data of longitudinal study ($n = 32$). *$P < 0.05$. **$P < 0.01$. ***$P < 0.001$.

the computer were analyzed with AIDA Image Analyzer 4.5 software (version 4.5; Raytest). The regions of interest were manually drawn on the FC, PTC, striatum, thalamus, and cerebellum following a Franklin and Paxinos mouse brain atlas. The regions of interest were analyzed as photostimulated intensity per square millimeter and presented as ratios to cerebellum.

Immunohistochemical Staining

The β-amyloid deposits were visualized using an antibody for $A\beta_{40}$-peptide (Anti-β-amyloid 1-40, rabbit polyclonal antibody; Millipore). Ionized calcium-binding adaptor molecule 1 (Iba1), an inflammation marker, is a microglia- and macrophage-specific calcium-binding protein. Iba1 was visualized with a specific Iba1 antibody (Wako Ltd.).

The fresh-frozen brain slides were thawed and fixed in 4% paraformaldehyde in phosphate-buffered saline, and the sections were incubated 10 min with 99% formic acid for the $A\beta_{40}$-staining. They then were incubated for 30 min with the blocking agent and subsequently for 48 h with the primary antibody (dilution of 1:400). After a wash with $1 \times$ phosphate-buffered saline + 0.3% Triton X-100, the slides were incubated for 1 h with the secondary antibody (biotin-goat anti-rabbit IgG [Invitrogen]; dilution of 1:400). An avidin–biotin complex kit (Vectastain Elite ABC-HRP Kit; Vector Laboratories) was used to effectively visualize the biotinylated antibodies in the stained tissues. The tissues were incubated with the avidin–biotin complex mix for 30 min followed by washing twice with 1× phosphate-buffered saline plus 0.3% Triton X-100 and once with only 1× phosphate-buffered saline. Finally, the brain sections were stained with Sigma*Fast* 3,3′-diaminobenzidine tablets (Sigma-Aldrich) to develop a brownish color that is resistant to alcohol. The slides were afterward dehydrated in an alcohol series, dipped in xylene, and mounted with distrene plasticizer xylene (DPX Mountant for histology; Sigma). Images of the stained slides were taken with a Panoramic 250 slide scanner (3DHISTECH).

Data Analysis and Statistics

The results are reported as average $\pm$ SD when n was at least 3. All statistical analyses were calculated using Prism programs (version 5.01; GraphPad Software). Differences in ^{11}C-PIB and ^{18}F-GE-180 binding between APP23 transgenic and WT animals were analyzed using the nonparametric Mann–Whitney U test because of the small sample size. Correlation between ^{11}C-PIB and ^{18}F-GE-180 binding was tested using the Pearson correlation coefficient. Differences were considered statistically significant if the P value was less than 0.05.

RESULTS

In Vivo ^{11}C-PIB and ^{18}F-GE-180 Imaging

The study was initiated as a pilot using 26-mo-old mice. Because significant differences were detected in these animals, a longitudinal study starting at 17 mo and continuing until 23 mo was initiated, and these results were combined with the pilot results. ^{11}C-PIB and ^{18}F-GE-180 showed a good brain penetration in the in vivo studies as observed in time–activity curves (Supplemental Fig. 2).

In vivo ^{11}C-PIB binding was clearly observed in cortical areas of transgenic mice (Fig. 1A). Ratios of FC, PTC, hippocampus, and thalamus to cerebellum in WT and transgenic mice at 17, 20, 23, and 26 mo were calculated. At 17 mo, the FC-to-cerebellum ($P < 0.01$), PTC-to-cerebellum ($P < 0.05$), and hippocampus-to-cerebellum ($P < 0.05$) ratios were already significantly higher in transgenic than in WT mice. These ratios increased significantly in transgenic mice until 26 mo, compared with WT mice ($P < 0.001$). The thalamus-to-cerebellum ratios were higher in transgenic than in WT mice only at 26 mo of age ($P < 0.001$) (Figs. 1B–1E).

In vivo ^{18}F-GE-180 PET binding was clearly observed in cortical areas of transgenic mice (Fig. 2A). At 17 mo, the FC-to-cerebellum
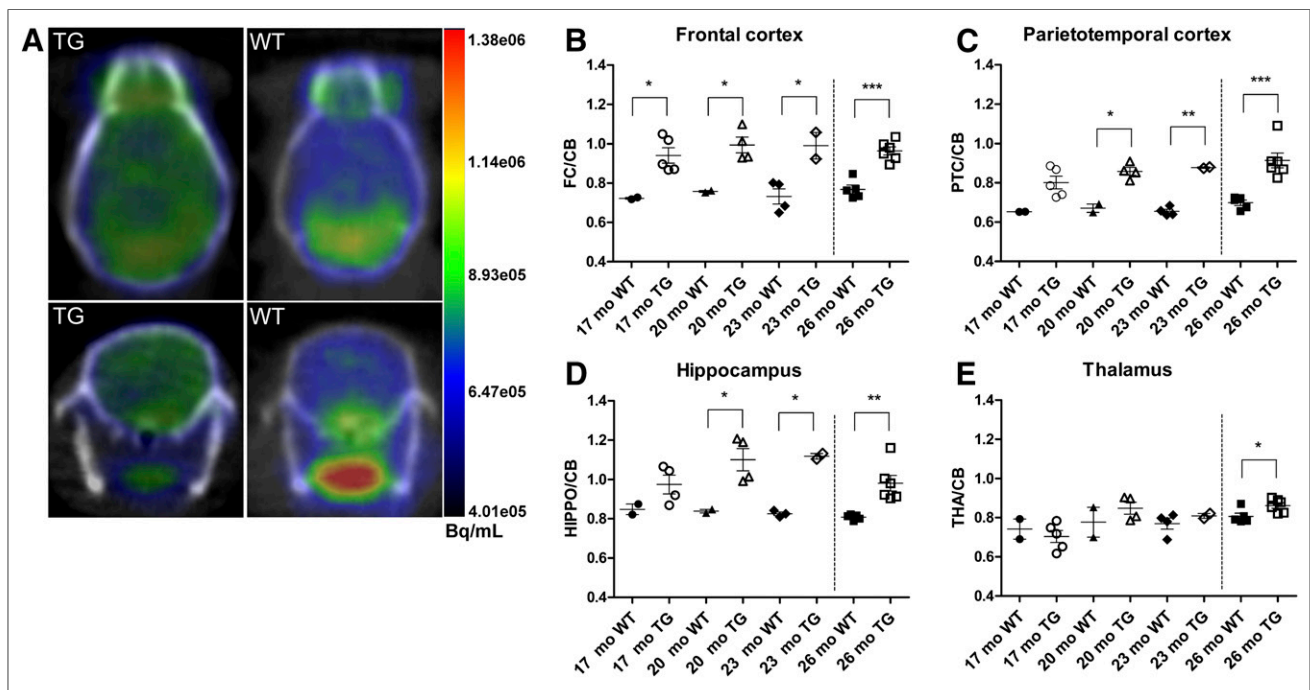

FIGURE 2. (A) In vivo PET images of ^{18}F-GE-180 in 26-mo-old transgenic (TG) and WT APP23 mice. (B–E) Ratios of FC (B), PTC (C), hippocampus (HIPPO) (D), and thalamus (THA) (E) to cerebellum (CB) from 17 to 26 mo of age. Dotted line separates data of pilot study from data of longitudinal study ($n = 30$). *$P < 0.05$. **$P < 0.01$. ***$P < 0.001$.
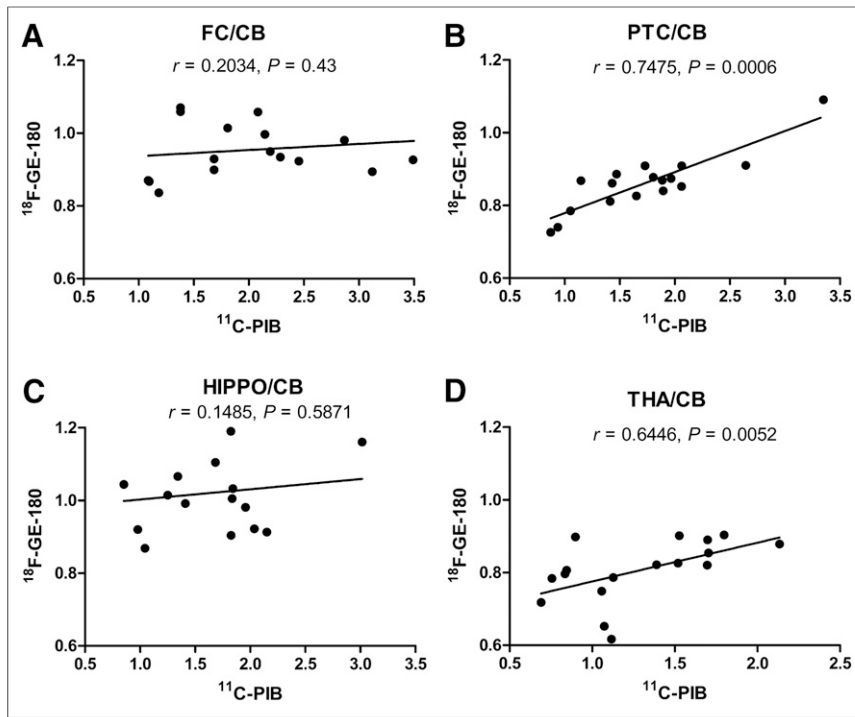
FIGURE 3. Correlation of the ratios of FC (A), PTC (B), hippocampus (HIPPO) (C), and thalamus (THA) (D) to cerebellum (CB) between ^{11}C-PIB and ^{18}F-GE-180 in transgenic APP23 mice from 17 to 26 mo of age, calculated with Pearson correlation ($n = 17$).

($P < 0.05$) and PTC-to-cerebellum ($P < 0.05$) ratios were already significantly higher in transgenic than in WT mice. These ratios increased significantly in transgenic mice until age 26 mo, compared with WT mice ($P < 0.001$). The hippocampus-to-cerebellum ratios were higher in transgenic than in WT mice starting at age 20 mo ($P < 0.01$), whereas the thalamus-to-cerebellum ratios were higher in transgenic than in WT mice only at age 26 mo ($P < 0.05$) (Figs. 2B–2E).

The correlation between ^{11}C-PIB and ^{18}F-GE-180 for the FC-to-cerebellum, PTC-to-cerebellum, hippocampus-to-cerebellum, and thalamus-to-cerebellum ratios in transgenic mice, combining all the studied time points, was subsequently calculated. Significant correlations were found between ^{11}C-PIB and ^{18}F-GE-180 binding for the PTC-to-cerebellum (Pearson $r = 0.7475$, $P = 0.0006$) and thalamus-to-cerebellum (Pearson $r = 0.6446$, $P = 0.0052$)

ratios. In contrast, the FC-to-cerebellum ($r = 0.2034$, $P = 0.43$) and hippocampus-to-cerebellum ($r = 0.1485$, $P = 0.5871$) ratios showed only a poor correlation (Fig. 3). Furthermore, we calculated the ratio and percentage increase from 17 to 20, 23, and 26 mo in the transgenic mice for ^{11}C-PIB and ^{18}F-GE-180, as shown in Table 1. In this table, we can observe that the ^{11}C-PIB percentage increase is progressive in all regions, reaching over a 100% increase for the FC-to-cerebellum, PTC-to-cerebellum, and hippocampus-to-cerebellum ratios and close to 100% for the thalamus-to-cerebellum ratio at 26 mo. The ^{18}F-GE-180 increases in the same period were much smaller, at 1% and 2% for the hippocampus-to-cerebellum and FC-to-cerebellum ratios, respectively, and 14% and 23% for the PTC-to-cerebellum and thalamus-to-cerebellum ratios at 26 mo.

Ex Vivo ^{11}C-PIB Binding and Immunohistochemistry

Autoradiographic images of 26-mo-old WT and transgenic ^{11}C-PIB–injected mice and immunohistochemical staining of $A\beta_{40}$ in the same transgenic mouse showed the colocalization of ^{11}C-PIB binding and $A\beta_{40}$-deposition in cortical areas, hippocampus, and thalamus. Neither specific ^{11}C-PIB binding nor $A\beta_{40}$-deposition could be detected in the cerebellum (Fig. 4A). FC-to-cerebellum ($P < 0.001$), PTC-to-cerebellum ($P < 0.001$), hippocampus-to-cerebellum ($P < 0.001$), and thalamus-to-cerebellum ($P < 0.01$) ratios were higher in transgenic than in WT mice (Fig. 4B).

Ex Vivo ^{18}F-GE-180 Binding and Immunohistochemistry

Autoradiographic images of 26-mo-old WT and transgenic ^{18}F-GE-180–injected mice and immunohistochemistry staining of Iba1 in the same transgenic mice showed colocalization of ^{18}F-GE-180 binding and Iba1 expression in cortical areas, hippocampus, and thalamus (Fig. 5A). FC-to-cerebellum, PTC-to-cerebellum, hippocampus-to-cerebellum ($P < 0.01$), and thalamus-to-cerebellum ($P < 0.05$) ratios

TABLE 1
Ratio and Percentage Increase from 17 to 20, 23, and 26 Months in APP23 Transgenic Mice

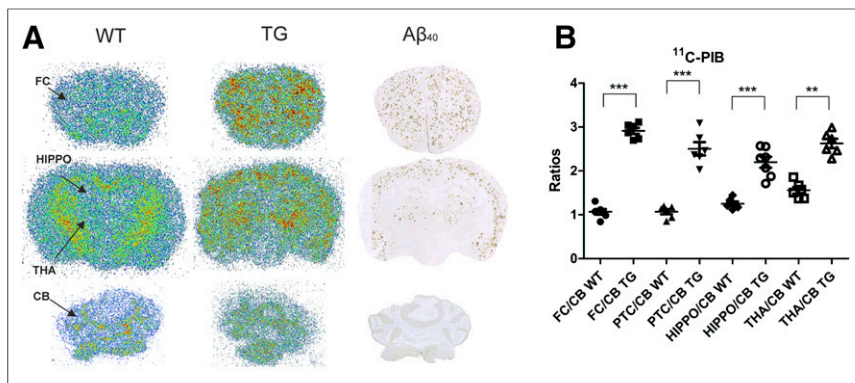| Site	^{11}C-PIB			^{18}F-GE-180		
	17–20 mo	17–23 mo	17–26 mo	17–20 mo	17–23 mo	17–26 mo
FC/CB	0.64 (52%)	1.03 (84%)	1.72 (140%)	0.00 (0%)	0.01 (1%)	0.02 (2%)
PTC/CB	0.56 (50%)	0.83 (75%)	1.13 (102%)	0.06 (8%)	0.08 (10%)	0.11 (14%)
HIPPO/CB	0.33 (30%)	0.70 (65%)	1.07 (100%)	0.03 (3%)	0.04 (4%)	0.01 (1%)
THA/CB	0.16 (17%)	0.24 (25%)	0.77 (82%)	0.03 (4%)	0.10 (14%)	0.16 (23%)

CB = cerebellum; HIPPO = hippocampus; THA = thalamus.

FIGURE 4. (A) Representative ex vivo autoradiography images of ^{11}C-PIB binding in 26-mo-old transgenic (TG) and WT APP23 mice together with Aβ$_{40}$-immunostaining (A). (B) Ratios of FC, PTC, hippocampus (HIPPO), and thalamus (THA) to cerebellum (CB). $**P < 0.01$. $***P < 0.001$.

were significantly higher in transgenic than in WT mice (Fig. 5B).

The increased ^{11}C-PIB and ^{18}F-GE-180 uptake in 26-mo-old transgenic versus WT mice in vivo and ex vivo was also compared (Supplemental Table 1). The in vivo and ex vivo results were similar for the cortical areas, whereas some variation was found in hippocampus and thalamus uptake between in vivo and ex vivo studies.

DISCUSSION

Although the findings from preclinical imaging studies cannot be directly extrapolated to humans, they are valuable when evaluating novel tracers and transgenic animal models and performing preclinical drug efficacy studies. Small-animal PET imaging of β-amyloid with ^{11}C-PIB has proved difficult, with major differences among AD animal models. The differences in the quantity and type of β-amyloid plaques has been suggested to be a key factor in ^{11}C-PIB binding in different animal models of AD, as shown by Snellman et al. (*10*), with APP23 mice having very high ^{11}C-PIB binding compared with the very low ^{11}C-PIB binding observed in Tg2576 and APPswe-PS1dE9 (APP/PS1) animals despite a similar total plaque load. For this reason, we decided to use the APP23 mouse model for this study.
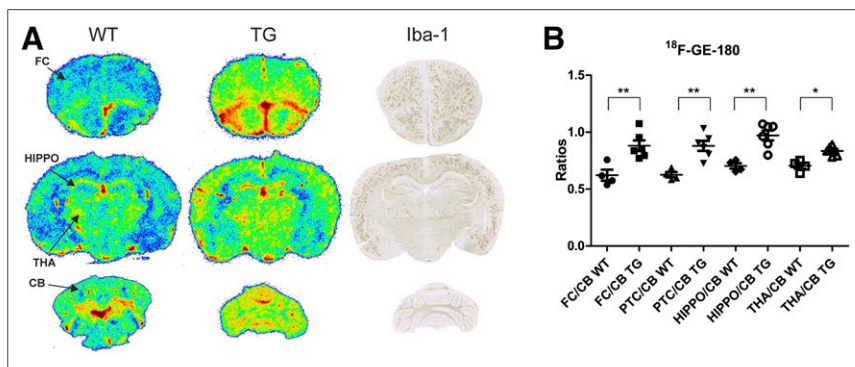

FIGURE 5. (A) Representative ex vivo brain autoradiography images of ^{18}F-GE-180 binding in 26-mo-old transgenic (TG) and WT APP23 mice together with Iba1 immunostaining. (B) Ratios of FC, PTC, hippocampus (HIPPO), and thalamus (THA) to cerebellum (CB). $*P < 0.05$. $**P < 0.01$.

^{11}C-PIB and ^{18}F-GE-180 In Vivo Binding Association

Here, we studied the association between β-amyloid deposition measured with ^{11}C-PIB and neuroinflammation measured with ^{18}F-GE-180 in the FC, PTC, hippocampus, and thalamus of APP23 transgenic mice from 17 to 26 mo of age. The results showed a good positive correlation between ^{11}C-PIB and ^{18}F-GE-180 binding ratios calculated for PTC and thalamus. In contrast, the obtained binding ratios for FC and hippocampus showed a poor correlation; whereas the ^{11}C-PIB binding ratios increased significantly over the time of the study in FC and hippocampus, a similar increase was not observed with ^{18}F-GE-180, as shown in Table 1. These results indicate a plateau of ^{18}F-GE-180 binding in the FC and hippocampus, regions where the β-amyloid deposition starts in this mouse model, whereas in the PTC and thalamus, ^{18}F-GE-180 binding continued to increase, matching the delayed β-amyloid deposition in these areas (*29*). Previously, Maeda et al. found a good correlation between the binding of an older TSPO tracer (^{11}C-AC5216) and increased age in the hippocampus of APP23 mice, but no correlation between the binding potentials of ^{11}C-AC5216 and ^{11}C-PIB in the same brain region (*14*). The difference with our study could be explained by the lack of a detectable TSPO increase with ^{11}C-AC5216 at very early stages of the disease (12–15 mo) and by the higher affinity of the ^{18}F-GE-180 used in the current study than of ^{11}C-AC5216. A recent clinical study with AD patients showed a clear ^{18}F-DPA-714 binding in ^{11}C-PIB–positive prodromal patients, without a further increase of the ^{18}F-DPA-714 binding in AD-demented patients (*30*). This outcome is in accordance with our current results showing no increase in ^{18}F-GE-180 binding in the FC and hippocampus.

^{11}C-PIB and ^{18}F-GE-180 Binding

In the current study, the ^{11}C-PIB binding ratios in the APP23 transgenic mice reached a value of between 2 and 3 at the older age groups in the cortical areas, in accordance with previous studies with the same mouse model (*6*). In similar studies using ^{18}F-AV-45 in APP/PS1 and APP/PS1-21 mice, however, the maximum ratio was approximately 1.1 (*31,32*), making the ratio increase in APP23 mice 20–30 times higher. These 3 mouse models have a similar amount of β-amyloid deposition in old age, but the types of plaque differ. The broad range of β-amyloid detection in the APP23 mouse with ^{11}C-PIB makes this combination of model and tracer a good choice for testing antiamyloid therapies.

Increased microglial activation has also been reported in postmortem brain samples of AD patients, although the role of microglia in AD is still controversial (*33,34*). In the APP23 animal model, previous studies have been performed with older TSPO

radiotracers, showing increased binding in the cortical regions (*14,35*). In the APP/PS1 model, increased neuroinflammation has been observed in 16- to 19-mo-old mice with ^{11}C-PK-11195 (*36*) whereas neuroinflammation was not detected in younger (13- to 15-mo-old) mice with ^{11}C-PK-11195 (*12*). Studies with ^{11}C-PBR28 have shown inflammation in the brains of 6-mo-old 5XFAD mice (*13*).

In addition to the ^{18}F-GE-180, used in this study, several ^{18}F-labeled TSPO tracers, such as ^{18}F-PBR06 and ^{18}F-DPA-714, have been used to detect neuroinflammation in different animal models of β-amyloid deposition. In vivo studies using ^{18}F-PBR06 differentiated 15- to 16-mo-old APP^{L/S} mice from age-matched WT mice (*15*) whereas longitudinal studies with ^{18}F-DPA-714 in APP/PS1 and APP/PS1-21 mouse models have shown increased TSPO tracer binding compared with WT littermates at different ages (*16,32*). Furthermore, recent studies have used ^{18}F-GE-180 to detect neuroinflammation in APP/PS1 and PS2APP mice (*17,23*).

Cerebellum as a Reference Region for Analysis

In our study, we used the cerebellum as the reference region for in vivo and ex vivo analyses of ^{11}C-PIB and ^{18}F-GE-180 binding. Use of the cerebellum as the reference region is well established for ^{11}C-PIB, but the choice is more controversial for analyzing the binding of TSPO tracers. Our use of the cerebellum as the reference region for ^{18}F-GE-180 was based on our PET imaging data showing no differences in ^{18}F-GE-180 SUVs in the cerebellum between transgenic and WT mice at any age (Supplemental Fig. 1).

It has been previously demonstrated that use of a pseudoreference region for TSPO tracer binding analyses increases the sensitivity of the PET analysis if no differences are found in the SUVs in the reference area (*37*). In 2 recent animal imaging studies, use of the cerebellum as a reference region decreased intragroup variability (*16,38*).

CONCLUSION

The neuroinflammation increase detected in the APP23 model using the TSPO radiotracer ^{18}F-GE-180 was relatively modest compared with the increase in β-amyloid detected with ^{11}C-PIB. Furthermore, the signal increase of ^{18}F-GE-180 plateaued at an earlier stage of pathogenesis, whereas the amyloidosis continued to increase. Given these findings, we suggest that TSPO-binding radiotracers are good tools for early pathogenesis detection in AD but might not be so suitable for long-term monitoring of disease progression.

DISCLOSURE

REFERENCES

1. Nordberg A, Rinne JO, Kadir A, Långström B. The use of PET in Alzheimer disease. *Nat Rev Neurol.* 2010;6:78–87.
2. Rinne JO, Brooks DJ, Rossor MN, et al. ^{11}C-PiB PET assessment of change in fibrillar amyloid-beta load in patients with Alzheimer's disease treated with bapineuzumab: a phase 2, double-blind, placebo-controlled, ascending-dose study. *Lancet Neurol.* 2010;9:363–372.
3. Klunk WE, Engler H, Nordberg A, et al. Imaging brain amyloid in Alzheimer's disease with Pittsburgh compound-B. *Ann Neurol.* 2004;55:306–319.
4. Scheinin NM, Aalto S, Kaprio J, et al. Early detection of Alzheimer disease: ^{11}C-PiB PET in twins discordant for cognitive impairment. *Neurology.* 2011;77:453–460.
5. Zwan MD, Rinne JO, Hasselbalch SG, et al. Use of amyloid-PET to determine cutpoints for CSF markers: a multicenter study. *Neurology.* 2016;86:50–58.
6. Maeda J, Ji B, Irie T, et al. Longitudinal, quantitative assessment of amyloid, neuroinflammation, and anti-amyloid treatment in a living mouse model of Alzheimer's disease enabled by positron emission tomography. *J Neurosci.* 2007;27:10957–10968.
7. Maier FC, Keller MD, Bukala D, et al. Quantification of β-amyloidosis and rCBF with Dedicated PET, 7 T MR imaging, and high-resolution microscopic MR imaging at 16.4 T in APP23 mice. *J Nucl Med.* 2015;56:1593–1599.
8. Maier FC, Wehrl HF, Schmid AM, et al. Longitudinal PET-MRI reveals β-amyloid deposition and rCBF dynamics and connects vascular amyloidosis to quantitative loss of perfusion. *Nat Med.* 2014;20:1485–1492.
9. Manook A, Yousefi BH, Willuweit A, et al. Small-animal PET imaging of amyloid-beta plaques with [^{11}C]PiB and its multi-modal validation in an APP/PS1 mouse model of Alzheimer's disease. *PLoS One.* 2012;7:e31310.
10. Snellman A, López-Picón FR, Rokka J, et al. Longitudinal amyloid imaging in mouse brain with ^{11}C-PiB: comparison of APP23, Tg2576, and APPswe-PS1dE9 mouse models of Alzheimer disease. *J Nucl Med.* 2013;54:1434–1441.
11. Stefaniak J, O'Brien J. Imaging of neuroinflammation in dementia: a review. *J Neurol Neurosurg Psychiatry.* 2016;87:21–28.
12. Rapic S, Backes H, Viel T, et al. Imaging microglial activation and glucose consumption in a mouse model of Alzheimer's disease. *Neurobiol Aging.* 2013;34:351–354.
13. Mirzaei N, Tang SP, Ashworth S, et al. In vivo imaging of microglial activation by positron emission tomography with [^{11}C]PBR28 in the 5XFAD model of Alzheimer's disease. *Glia.* 2016;64:993–1006.
14. Maeda J, Zhang MR, Okauchi T, et al. In vivo positron emission tomographic imaging of glial responses to amyloid-beta and tau pathologies in mouse models of Alzheimer's disease and related disorders. *J Neurosci (Online).* 2011;31:4720–4730.
15. James ML, Belichenko NP, Nguyen TV, et al. PET imaging of translocator protein (18 kDa) in a mouse model of Alzheimer's disease using *N*-(2,5-dimethoxybenzyl)-2-^{18}F-fluoro-*N*-(2-phenoxyphenyl)acetamide. *J Nucl Med.* 2015;56:311–316.
16. Takkinen JS, López-Picón FR, Al Majidi R, et al. Brain energy metabolism and neuroinflammation in ageing APP/PS1-21 mice using longitudinal ^{18}F-FDG and ^{18}F-DPA-714 PET imaging. *J Cereb Blood Flow Metab.* 2016:271678X16677990.
17. Liu B, Le KX, Park MA, et al. In vivo detection of age- and disease-related increases in neuroinflammation by ^{18}F-GE180 TSPO microPET imaging in wild-type and Alzheimer's transgenic mice. *J Neurosci.* 2015;35:15716–15730.
18. Wadsworth H, Jones PA, Chau WF, et al. [^{18}F]GE-180: a novel fluorine-18 labelled PET tracer for imaging translocator protein 18 kDa (TSPO). *Bioorg Med Chem Lett.* 2012;22:1308–1313.
19. Boutin H, Murray K, Pradillo J, et al. ^{18}F-GE-180: a novel TSPO radiotracer compared to ^{11}C-R-PK11195 in a preclinical model of stroke. *Eur J Nucl Med Mol Imaging.* 2015;42:503–511.
20. Sridharan S, Lepelletier FX, Trigg W, et al. Comparative evaluation of three TSPO PET radiotracers in a LPS-induced model of mild neuroinflammation in rats. *Mol Imaging Biol.* 2017;19:77–89.
21. Dickens AM, Vainio S, Marjamäki P, et al. Detection of microglial activation in an acute model of neuroinflammation using PET and radiotracers [11]C-(*R*)-PK11195 and ^{18}F-GE-180. *J Nucl Med.* 2014;55:466–472.
22. Airas L, Dickens AM, Elo P, et al. In vivo PET imaging demonstrates diminished microglial activation after fingolimod treatment in an animal model of multiple sclerosis. *J Nucl Med.* 2015;56:305–310.
23. Brendel M, Kleinberger G, Probst F, et al. Increase of TREM2 during aging of an Alzheimer's disease mouse model is paralleled by microglial activation and amyloidosis. *Front Aging Neurosci.* 2017;9:8.
24. Feeney C, Scott G, Raffel J, et al. Kinetic analysis of the translocator protein positron emission tomography ligand [^{18}F]GE-180 in the human brain. *Eur J Nucl Med Mol Imaging.* 2016;43:2201–2210.

25. Wickstrøm T, Clarke A, Gausemel I, et al. The development of an automated and GMP compliant FASTlab™ Synthesis of [^{18}F]GE-180; a radiotracer for imaging translocator protein (TSPO). *J Labelled Comp Radiopharm.* 2014;57: 42–48.

26. Sturchler-Pierrat C, Abramowski D, Duke M, et al. Two amyloid precursor protein transgenic mouse models with Alzheimer disease-like pathology. *Proc Natl Acad Sci USA.* 1997;94:13287–13292.

27. Calhoun ME, Wiederhold K, Abramowski D, et al. Neuron loss in APP transgenic mice. *Nature.* 1998;395:755–756.

28. Databases: overview. MRM NeAt (Neurological Atlas) Mouse Brain Database website. http://brainatlas.mbi.ufl.edu/Database/. Released August 11, 2005. Accessed November 9, 2017.

29. Sturchler-Pierrat C, Staufenbiel M. Pathogenic mechanisms of Alzheimer's disease analyzed in the APP23 transgenic mouse model. *Ann N Y Acad Sci.* 2000; 920:134–139.

30. Hamelin L, Lagarde J, Dorothée G, et al. Early and protective microglial activation in Alzheimer's disease: a prospective study using ^{18}F-DPA-714 PET imaging. *Brain.* 2016;139:1252–1264.

31. Poisnel G, Dhilly M, Moustié O, et al. PET imaging with [^{18}F]AV-45 in an APP/PS1-21 murine model of amyloid plaque deposition. *Neurobiol Aging.* 2012;33: 2561–2571.

32. Sérrière S, Tauber C, Vercouillie J, et al. Amyloid load and translocator protein 18 kDa in APPswePS1-dE9 mice: a longitudinal study. *Neurobiol Aging.* 2015;36: 1639–1652.

33. Heneka MT, Carson MJ, El Khoury J, et al. Neuroinflammation in Alzheimer's disease. *Lancet Neurol.* 2015;14:388–405.

34. Prokop S, Miller KR, Heppner FL. Microglia actions in Alzheimer's disease. *Acta Neuropathol (Berl).* 2013;126:461–477.

35. Ji B, Maeda J, Sawada M, et al. Imaging of peripheral benzodiazepine receptor expression as biomarkers of detrimental versus beneficial glial responses in mouse models of Alzheimer's and other CNS pathologies. *J Neurosci.* 2008;28:12255–12267.

36. Venneti S, Lopresti BJ, Wiley CA. The peripheral benzodiazepine receptor (translocator protein 18kDa) in microglia: from pathology to imaging. *Prog Neurobiol.* 2006;80:308–322.

37. Lyoo CH, Ikawa M, Liow JS, et al. Cerebellum can serve as a pseudo-reference region in Alzheimer disease to detect neuroinflammation measured with PET radioligand binding to translocator protein. *J Nucl Med.* 2015;56:701–706.

38. Brendel M, Probst F, Jaworska A, et al. Glial activation and glucose metabolism in a transgenic amyloid mouse model: a triple-tracer PET study. *J Nucl Med.* 2016;57:954–960.